DOI: 10.1002/chem.200801045

Effect of Doped Transition Metal on Reversible Hydrogen Release/Uptake from $NaAlH_4$

Jianjun Liu, You Han, and Qingfeng Ge*[a]

Abstract: Periodic density functional theory calculations with plane-wave basis set and projector-augmented wave potentials have been carried out to investigate the stability and hydrogen interaction in the $NaAlH_4$(001) surfaces doped with 3d transition-metal (TM) elements. A complex structure, $TMAl_3H_{12}$, in which the TM atom occupies the interstitial position formed from three AlH_4^- groups, is the most stable structure for TM = Sc to Co. The stability of the complex structure, as well as the hydrogen desorption energies from different positions of the complex structure, was found to follow the 18-electron rule in general. The electron-deficient $TMAl_3H_x$ tends to get more electrons by coordinating with the surrounding Al–H bonds and H–H bond, or by losing the "outside" hydrogen atoms. On the other hand, the electron-rich complex loses its excess electrons easily by releasing AlH_x, which resulted in the formation of a new catalytic center, or by desorbing H_2. By cycling between the electron-deficient and electron-rich states, $TMAl_3H_x$ acted as an active center in reversible hydrogen release/uptake processes. Electronic structure analysis revealed that the electron transfer between hydrogen and Al groups mediated by the d orbitals of TMs played important roles in hydrogen release/uptake from alanate-based materials. The exchange of ligands can be described as a σ-bond metathesis process catalyzed by transition metals through a dihydrogen complex. Early transition metals are more efficient to reduce hydrogen desorption energy and break H–H and Al–H bonds as a result of balanced electron-accepting/backdonating abilities, making them better candidates as catalysts. The present analyses are consistent with the experimental observations.

Keywords: catalysis · density functional calculations · dihydrogen complexes · electron counting · hydrogen storage

Introduction

A hydrogen economy has the benefits of achieving long-term energy security and minimizing environmental hazards but its implementation faces many technical barriers. One such barrier is the lack of lightweight, high-density, low-cost hydrogen storage technologies.[1,2] Over the past decades, many advanced materials including complex metal hydrides,[3] chemical hydrides,[4,5] and metal–organic frameworks[6–8] have been explored as potential on-board hydrogen storage candidates. In particular, the lightweight complex metal hydrides ($MAlH_4$ and MBH_4, M: alkali metal) enhanced by 3d-transition metal (TM) compounds offer a promising opportunity as solid-state hydrogen storage media for transportation applications due to Bogdanovic and Schwickardi's breakthrough discovery with Ti-doped $NaAlH_4$.[9] The discovery stimulated a large number of studies aimed at unraveling the role played by Ti as well as the mechanism of hydrogen adsorption and desorption in Ti-catalyzed $NaAlH_4$. Great efforts have also been devoted to reduce the hydrogen release and recharging temperatures by improving the kinetics of the $NaAlH_4$-based systems.[10–17] A recyclable hydrogen capacity of about 4 wt% in Ti-doped $NaAlH_4$ has been achieved routinely with reasonably good kinetics below the melting point.[18–20] Although the hydrogen capacity of the Ti-doped $NaAlH_4$ would not meet the target set by the US Department of Energy, the system serves as a useful prototype to understand the hydrogen interaction in similar complex metal hydrides. Understanding the origin of the enhanced hydrogen cyclic property by doping Ti in $NaAlH_4$ is expected to be helpful in the design of new hydrogen storage materials with much improved performance.[3,21–28]

[a] Dr. J. Liu, Y. Han, Prof. Dr. Q. Ge
Department of Chemistry and Biochemistry
Southern Illinois University
Carbondale, IL, 62901 (USA)
Fax: (+1) 618 453 6408
E-mail: qge@chem.siu.edu

Supporting information for this article is available on the WWW under http://dx.doi.org/10.1002/chem200801045.

Clearly, catalysts are essential in systems that store hydrogen chemically to meet the demand of transportation application. In Al- or B-based complex hydrides, the catalyst should weaken the Al–H or B–H bonds by either interacting with H directly or through the Al (B) atom, whereas the nascent bonds formed between the catalyst and hydrogen should not be too strong to prevent hydrogen from combining to form molecular hydrogen and desorbing from the system. During the recharging phase, the catalyst should assist in breaking the molecular hydrogen bond but not prevent the hydrogen atoms from migrating to Al (B) sites. Consequently, the hydrogen atoms formed from the dissociation at the active site will be mobile enough to be transferred to the surrounding host atoms. An ideal catalyst should provide a balanced effect on hydrogen interaction for hydrogen desorption and adsorption in the complex metal hydrides.

In the search for catalysts with the highest performance for hydrogen release/uptake in complex metal hydrides, particularly in $NaAlH_4$, extensive studies have been carried out by examining the effect of adding various metal compounds including 3d-TM elements as well as Zr, Ag, Cd, Ce.[19,29] These investigations demonstrated that $TiCl_3$ was the best among the compounds examined at achieving rapid hydrogen release. Very recently, $NaAlH_4$ ball-milled with $ScCl_3$ was shown to exhibit even better cyclic property and kinetics than $TiCl_3$ at the same level.[30,31] The results of $ScCl_3$-doped $NaAlH_4$ are consistent with the general conclusion that 3d TMs from left to right in the periodic table exhibit diminishing catalytic reactivity and the cationic radius could be used as an indicator of dehydrogenation activity.[29] On the other hand, the underlying origin that determines the catalytic activity of the dopants in $NaAlH_4$ remains unclear.

Previously, we predicted an interstitial $TiAl_3H_{12}$ complex structure to be the most stable species in both Ti-doped $NaAlH_4$(001) and (100) surfaces based on density functional theory (DFT) slab calculations.[32,33] Our prediction of the complex structure was confirmed by a recent experimental study: the interstitial structure was shown to account for 75% of all Ti doped in $NaAlH_4$.[34] Our previous results also showed that hydrogen desorption energies from many positions of the $TiAl_3H_{12}$ complex structure were reduced considerably as compared with that from an undoped clean surface. We further demonstrated that the formation of $TiAl_3H_x$ not only promoted dehydrogenation locally from the complex but also had an extended effect on the surrounding AlH_4^- units by reducing the hydrogen desorption energy in the extended structure or by transferring hydrogen to the local complex structure. On the other hand, many other computational studies have been based on the bulk $NaAlH_4$ structure and focused on the substitutional mode of doping, that is, replacing either Na or Al with Ti.[28,35,36] Araujo et al. suggested that the thermodynamic stability of metal hydrides can be changed by this substitution. Titanium is less metallic than either Na or Li. Consequently, Ti has a lower ability to donate its electrons than Na and Li. As such, the Al–H bonds in the tetrahedral structure will be weakened due to electron-deficiency after Li or Na was substituted by Ti. According to these arguments, however, the late 3d TMs (Fe, Co, Ni, Cu, Zn) would be more efficient at weakening the Al–H bonds due to the even lower ability of donating electrons, contrary to the experimental observations of doping various TMs in $NaAlH_4$.[29]

The geometrical and electronic structure of the active site can be as important as the intrinsic chemical interaction in the catalytic complex in controlling the overall performance of the catalyst. For a system involving TM elements, the 18-electron rule was evoked to explain the stability of the complexes with different ligands.[37] The discovery by Kubas and co-workers of the tungsten complex with an η^2-bound H_2 ligand[38] as well as its generalization to other σ bonds as ligands has led to the identification of a large number of complexes.[39,40] The concept has also been exploited in searching for and designing new hydrogen storage candidates computationally.[41] The maximum number of hydrogen molecules absorbed by a conjugated compound-bound TM in a Kubas complex has been shown to be consistent with the 18-electron rule.[42–46] Kiran et al. extended such concepts to interactions between transition metals and organic molecules such as C_4H_4, C_5H_5, and C_8H_8 in their design of hydrogen storage materials.[47]

The previously reported dihydrogen or σ-bond complexes are molecular complexes.[39] With the identification of the $TiAl_3H_{12}$ complex structure in a periodic DFT calculation, we would generalize the dihydrogen and σ-bond as ligands of a complex to the extended systems found in a solid-state environment. Accordingly, dehydrogenation and rehydrogenation reactions in Ti-doped $NaAlH_4$ can be viewed as the exchange of σ-bond ligands: Al–H and H–H. The dihydrogen complexes with co-ligands will allow us to explore the catalytic mechanism by homolytic or heterolytic σ-bond activation at the TM center.

Herein, we report a systematic study of 3d-TMs (Sc, Ti, V, Cr, Mn, Fe, Co, Ni) doped in the $NaAlH_4$(001) surface. The structures and energetics of Sc- and Ti-doped $NaAlH_4$ have been reported previously.[32,33,48] Here, we combine them with the new results for the remaining 3d TMs and hope to unravel the effect of dopants on hydrogen interaction in $NaAlH_4$ by comparing the geometry and energetics as well as by examining the changes in electronic structure. In particular, we will examine the σ-bond interaction with the doped TMs and explore its role in stabilizing the complex as well as catalyzing dehydrogenation and rehydrogenation. The approach and understanding can be applied in the search for a more efficient catalyst for other high capacity complex hydrides such as $LiBH_4$, $LiAlH_4$, and $Mg(AlH_4)_2$.

Results and Discussion

Structural stability and its correlation with the eighteen-electron rule: The preferred sites of Ti in $NaAlH_4$ have been a central issue of many theoretical investigations. The conclusion often depends on the doping model as well as the refer-

ence states of elements involved. Many previous theoretical studies have been performed by doping Ti in the $NaAlH_4$ bulk structure.[28,35,49] Only a few studies adopted the surface models.[28,50] Even in those studies, only substitutional doping modes were examined. In our studies, we chose the $NaAlH_4$ surfaces and explored different doping modes on the basis of the surface model. Our selection of the surface-based models was based on the fact that hydrogen release/uptake in the $NaAlH_4$-based materials has to be achieved through the particles constantly exposing their surfaces.

In the previous study, we explored a series of possible positions for Ti when Ti was doped in $NaAlH_4$(001) and $NaAlH_4$(100).[32,33] These possible positions resulted in six structures. We grouped these six structures into three types of interaction modes: 1) Ti occupies the interstitial site formed from three AlH_4^- units of the first and second layers; 2) Ti is adsorbed on the surface and connecting with H or Al atoms; 3) Ti substitutes the Na atom in the lattice and pushes the Na atom either down into bulk or up on the surface. These interaction modes from Ti were used as a template in the subsequent studies of other TMs, including Sc, V, Cr, Mn, Fe, Co, Ni. The initial structures of doping other 3d elements were constructed by replacing Ti with the element of interest. The structure was then allowed to optimize self-consistently.

In our calculations, the relative stability of different doping modes does not depend on the reference state for an individual TM. However, the reference states (bulk or atom) of TMs will affect the relative binding energies when the binding energies of different TMs are compared. Herein we chose the bulk state of each TM as the reference state based on the fact that the bulk states are the standard thermodynamic state. The binding energies were calculated according to Equation (1):

$$E_{bind} = E_{tot}(\text{TM-NaAlH}_4) - E_{tot}(\text{NaAlH}_4) - E_{tot}(\text{TM}) \quad (1)$$

where E_{tot}(TM-$NaAlH_4$), E_{tot}($NaAlH_4$), and E_{tot}(TM) are the total energies of the relaxed TM-doped $NaAlH_4$(001) surface, the clean $NaAlH_4$(001) surface, and the bulk TM, respectively.

The binding energy for each TM doped in the $NaAlH_4$-(001) surface was plotted in Figure 1. We note that all binding energies are positive, indicating that energy has to be supplied to force the TM atom into different positions. This energy may be provided through ball-milling or other doping techniques prior to hydrogen release/uptake cycles. During hydrogen cycles, Ti, as well as other TMs, seem to favor the phase-separated bulk structure as indicated in Figure 1. However, a highly dispersed and more stable Ti–Al alloy phase on the surface of Al particles has been observed after dehydrogenation.[23,24,51] The phase-separation of forming a bulk-like TM may occur and lead to the loss of hydrogen cycling capacity in the long term, which is consistent with the experimental observation.[9,14] We also note that binding energies of the two structures in the same doping mode follow a similar trend. For example, the binding energy of **Inter_1** follows that of **Inter_2** from left to right of the periodic table. On the other hand, the binding energy of surface adsorption modes (**Surf_1** and **Surf_2**) varies differently from that of the interstitial modes (**Inter_1** and **Inter_2**). Similar to Ti-doped $NaAlH_4$(001) and (100),[32,33] the interstitial structures are more stable than the structures resulting from other doping modes for Sc–Co. Only in the case of doping Ni, the surface adsorption mode becomes more stable. Figure 1 also shows that the energy required for forming the interstitial structure decreases from Sc to Cr, and then increases slightly from Cr to Co. Consequently, both early and late TMs (Sc, Ti, Co, Ni) show weaker binding with $NaAlH_4$(001) than the middle TMs (Cr, Mn, and Fe) in the interstitial doping modes.

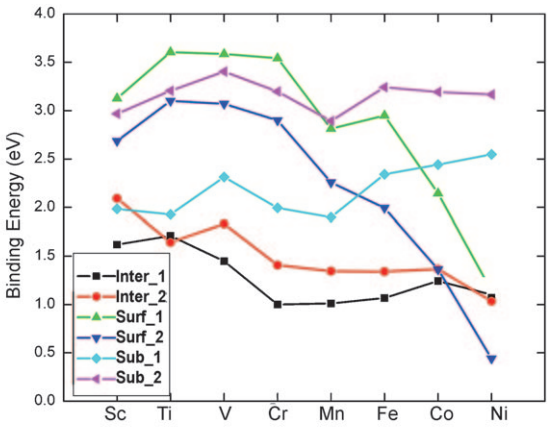

Figure 1. DFT-PBE binding energies of 3d TMs doped in $NaAlH_4$(001) surface with different doping modes. The bulk state of the transition metal was used as reference.

The difference in stabilities between the interstitial and surface structures can be understood by correlating the ligand number of the TM with the 18-electron rule. As indicated in the Introduction, both Al–H and H–H σ bonds can be considered as ligands, following Kubas' generalization.[39] Therefore, there are four Al–H ligands in the surface adsorption structure discussed above, whereas six Al–H ligands interact with TMs in the interstitial structure. The total number of electrons available to the TM can be counted as given in Equation (2):

$$N_{te} = N_{ve} + 2 \times N_{le} \quad (2)$$

where N_{te}, N_{ve}, and N_{le} are the total number of electrons, the number of valence electrons, and the number of Al–H ligands, respectively. An Al–H bond was considered to contribute two electrons to the TM whether the bond remained intact or was broken. We should point out that the high-spin state of the complex makes it coordinate with less ligands because of singly occupied orbitals. Furthermore, the infinite nature of the periodic system makes a quantitative comparison with a traditional complex difficult. However, we do hope to demonstrate that a qualitative picture with regard

to the relative stability of various doping modes emerges based on the 18-electron rule.

Among the TM complexes, $CrAl_3H_{12}$ ($N_{ve}=6$, $N_{le}=6$) is the most stable. The early or late TM complexes show weaker binding because of either electron deficiency ($N_{te}<18$) or excess ($N_{te}>18$) with respect to 18 electrons required by TMs. The stability of the surface adsorption structures, with four Al–H ligands, increases with the increasing number of d electrons, in agreement with the 18-electron rule. The surface structure formed with Ni, with two AlH_4^- units and each contributing two Al–H ligands, is the most stable, which is consistent with the fact that there are exactly 18 electrons in the surface complex formed with Ni. The ligand and electron counting in the substitutional structures are not straightforward. However, a general trend of decreasing the number of Al–H ligands was still observed in those structures. Similar analysis can be applied to other Al- and B-based complex hydrides such as $LiAlH_4$, $Be(AlH_4)_2$, $LiBH_4$, and $Be(BH_4)_2$. All these hydrides have been considered as promising hydrogen storage materials.

$TMAl_3H_{12}$—Geometrical and electronic structures: To further understand the interaction between the TM atom and surrounding $NaAlH_4$, we explored the geometrical and electronic structures based on the most stable interstitial $TMAl_3H_{12}$ structure, **Inter_1**. Figure 2 shows the variation of

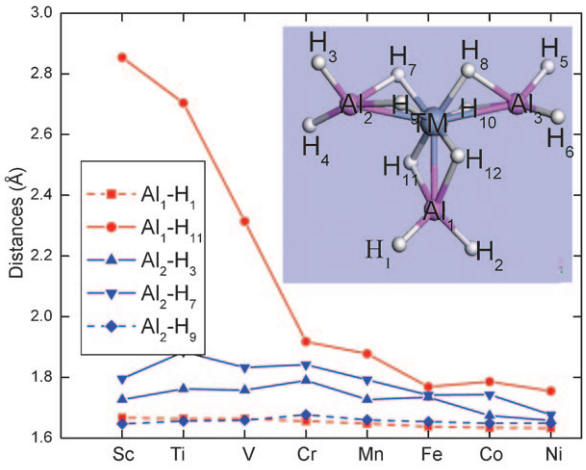

Figure 2. Variation of Al–H bond lengths in $TMAl_3H_{12}$ with TM. The Al and H atoms are numbered as in the structural model shown in the inset.

bond lengths as a function of TM. A schematic structural model was included in the inset of Figure 2 to label the atoms and to show the corresponding bonds. As shown in the schematic model, $TMAl_3H_{12}$ possesses C_2 symmetry, and the two Al atoms, Al_2 and Al_3, are equivalent. As such, we only show the results of TM interacting with the Al_1 group (Al_1, H_1, H_2, H_{11}, H_{12}) and the Al_2 group (Al_2, H_3, H_4, H_7, H_9). We grouped the hydrogen atoms in the local structure into two groups: outside (H_{1-6}) and inside (H_{7-12}) hydrogen. As shown in Figure 2, early TMs (Sc–V) interact more strongly with the Al_1 group than with the Al_2 group, manifested by the fact that the Al_1–H_{11} and Al_1–H_{12} bonds (from the Al_1 group) were completely broken, whereas the Al_2–H_7 and Al_2–H_9 bonds were elongated but remained bonded. The major decrease in the Al_1–H_{11} distance occurs from $ScAl_3H_{12}$ (2.854 Å) to $CrAl_3H_{12}$ (1.918 Å). From $CrAl_3H_{12}$ to $NiAl_3H_{12}$, the Al_1–H_{11} distance was only changed by 0.160 Å from 1.918 to 1.755 Å. The decrease is accompanied by an increase in the number of d electrons in the TM. In the $TMAl_3H_{12}$ structure formed with Sc and Ti, two original Al–H bonds (Al_1–H_{11} and Al_1–H_{12}) were completely broken, and the dissociated H atoms (H_{11} and H_{12}) were displaced from Al_1 to being shared by Al_2 (or Al_3) and the TM. The detailed structural information for Sc and Ti interstitial complex structures can be found in our previous publications.[32,3348] Vanadium also caused the Al_1–H_{11} and Al_1–H_{12} bonds to break. The two dissociated H atoms (H_{11} and H_{12}) are only bound to V. As we move further to Cr and Mn, the Al_1–H_{11} and Al_1–H_{12} bonds can only be considered partially broken, with distances of 1.918 and 1.878 Å, respectively. These two H atoms (H_{11} and H_{12}) are situated between the TM atom and Al_1, forming TM–H–Al_1 bridging structures. In the complexes formed with Fe, Co, and Ni, the Al_1–H_{11} and Al_1–H_{12} bonds remained intact. They were elongated by less than 0.2 Å with respect to the Al–H bond length of 1.643 Å in the undisturbed tetrahedral AlH_4^- group.

The energetics and structures of the TM interaction with Al–H bonds can be further analyzed by the donation and backdonation model originally proposed by Dewar, Chatt, and Duncanson (DCD).[52,53] This model has been applied extensively to the description of the interaction between a TM and ligands in an organometallic complex.[54–57] The local density of states (LDOSs) of **Inter_1** are shown in Figure 3, in which the plots are arranged in the order of Sc, Ti, V, Cr, Mn, Fe, Co, Ni from top to bottom. In all DOS calculations, we used the default atomic radii in the PAW potentials. Figure 3a shows the LDOSs projected onto each TM. Evidently, the main contribution to the LDOSs was from the 3d states of TMs. The contributions from the s and p states are negligible. In Figure 3b and c, LDOSs projected onto the Al atoms (Al_1 and Al_2) were plotted. We also included schematics of the molecular orbitals that associated with the energy ranges between the two vertical lines in each plot in the LDOSs.

Generally, electron donation occurs from the highest occupied orbital of Al–H bonds to the empty d orbitals of the TM. The calculated energies of the d states of TMs usually span the range from −2 to 2 eV. In the LDOSs of TMs doped in the $NaAlH_4$(001) surface, some new states, however, appear in the energy range of −4 to −6 eV, as shown in Figure 3a. These new states were attributed to the interaction between Al–H bonding states and metal d orbitals. The electron transfer from the Al–H bonding states to the empty d orbitals occurred due to the orbital overlap between the TM and the inner hydrogen atoms. This electron transfer weakened the Al–H bond and caused the elonga-

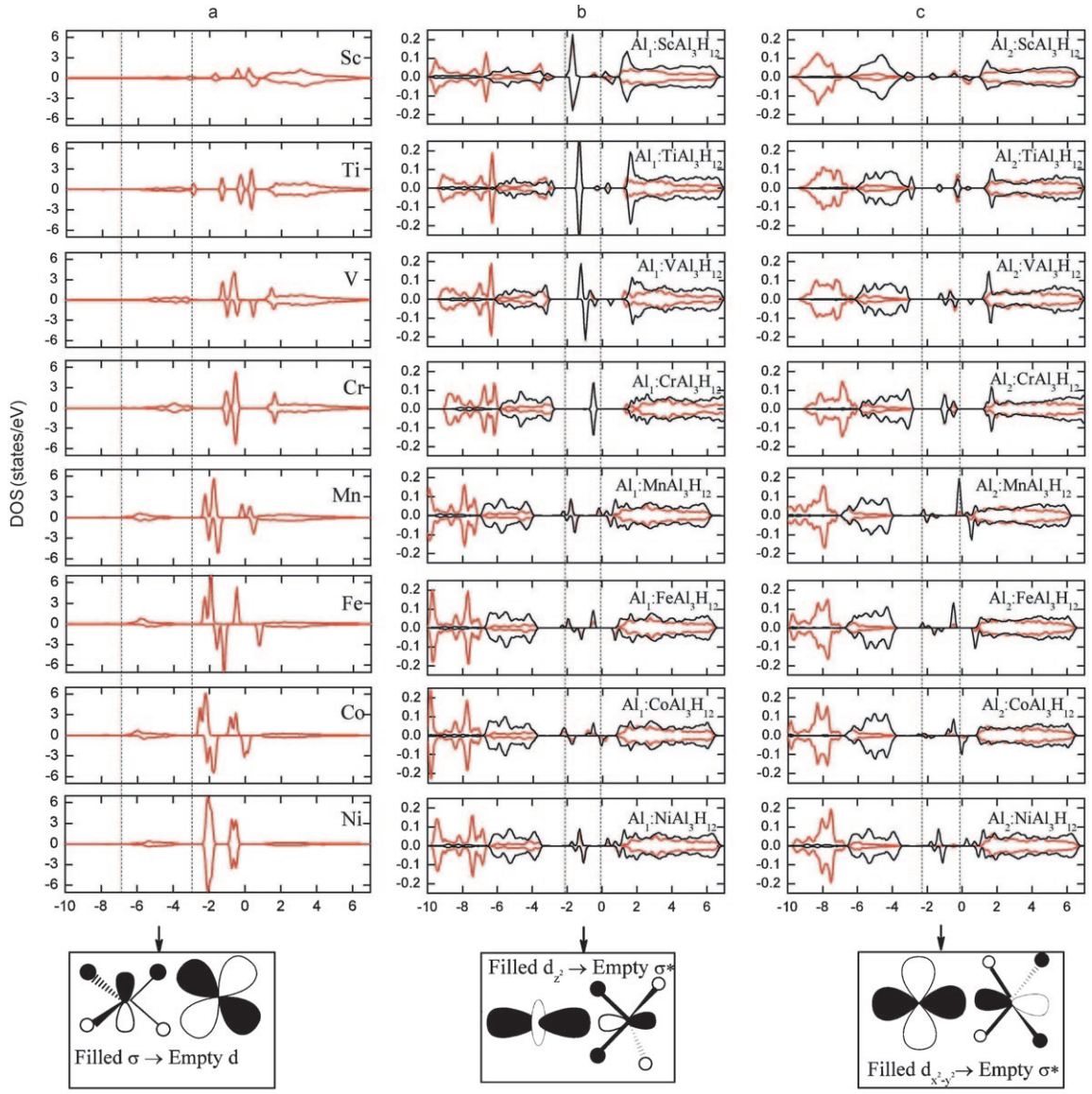

Figure 3. Local density of states (LDOS) of TM (a), Al_1 (b), and Al_2 (c) in $TMAl_3H_{12}$ with TM = Sc, Ti, V, Cr, Mn, Fe, Co, and Ni. Spin-up (positive) and spin-down (negative) densities were plotted. The molecular orbitals contributing to the states in the energy range between the dash lines were schematically shown underneath the corresponding LDOS plot. The atoms were numbered according Figure 2.

tion/breaking of inner Al–H bonds. On the other hand, the electron backdonation occurred from the filled d orbitals of TMs to the empty σ* orbitals of Al–H bonds, as illustrated in the LDOSs projected on Al_1 and Al_2 (Figure 3b and c). In a normal tetrahedral AlH_4^- group without TM, there was no peak in the energy range of −2 to 0 eV.[58] In contrast, new peaks appeared in the energy range of −2 to 0 eV in the LDOSs of the Al atoms. These new peaks originated from the interaction between the empty σ* orbitals of AlH_4^- units and the occupied TM d orbitals. The extent of the backdonation depends on the energy difference between the lowest unoccupied σ* orbitals of the Al–H bonds and the highest occupied d orbitals of the TM. A smaller energy difference would provide a better chance for the orbital to overlap and increase the backdonations. The intrinsic properties of a metal such as the filling and width of the d-band are therefore expected to affect the backdonation of TM. The energy difference increases with the increasing number of d electrons, since the d-band center is shifted to a lower energy.[59] Consequently, the early TMs exhibit a better electron backdonation ability than the late ones, as shown in Figure 3b and c. The decreasing backdonation from Sc to Ni may be correlated with the corresponding ionization potential. Strong backdonation from the TM to the Al_1–H bonds caused the bonds to break and displaced the H atoms (H_{11} and H_{12}) from Al_1, resulting in the H atoms (H_{11} and H_{12}) being shared by $Al_2(Al_3)$ and TM (see Figure 2). Consequently, the hydrogen desorption rate from TM-doped $NaAlH_4$ would decrease as the TM was changed from Sc to Ni. This is consistent with the experimental observation that

doping early 3d TMs led to a faster hydrogen desorption rate than doping the late ones.[29] The geometrical arrangement between the TM and the ligands also affects the back-donation. As shown in Figure 3b and c, the doped TM interacts stronger with the Al_1 group than with the other two AlH_4^- groups, especially for the early TMs (Sc, Ti, V). Orbital analysis shows that the d_{z^2} orbital of the TM overlaps with the σ* orbital of the Al_1 group, which was a combination of a p_z orbital of Al_1 and an s orbital of the associated H atoms. Such interactions are related to the geometrical arrangement and symmetry, including orbital symmetry, which is important in determining which direction would maximize the orbital overlap.

Based on the analysis of the interstitial structures in the TM-doped $NaAlH_4$(001) surface, we conclude that a combination of the number of valence electrons and the number of Al–H ligands determines the stability of the structure. The occupation of d orbitals increases, whereas the spatial distribution of d-electron density decreases from left to right in the periodic table. These intrinsic properties determine the mode as well as the strength of the TM–complex hydride interactions.

Hydrogen desorption catalyzed by transition metals: We previously reported that the interstitial complex structures formed with Sc and Ti not only are the most stable structures but also reduce the hydrogen desorption energies as compared with that from clean, undoped $NaAlH_4$ surfaces.[32,33,48] This effect of reducing hydrogen desorption energies was also extended to the surrounding AlH_4^- units. The effect of doping other TMs on hydrogen desorption energy has been examined in the present study. Similarly, the desorption energy of hydrogen was defined as given in Equation (3),

$$\Delta E_{des} = E_{stoi} - E_{H_2} - E_{Hdes} \quad (3)$$

where E_{stoi}, E_{Hdes}, and E_{H_2} are total energies of stoichiometric slab, the slab with H desorbed, and one H_2 molecule, respectively. This expression gives the energy cost of forming one hydrogen molecule in the gas phase by removing two hydrogen atoms from the slabs and is closely correlated with the experimentally measured heats of hydrogen desorption based on hydrogen isotherms. Figure 4 shows the variation of hydrogen desorption energy in $TMAl_3H_{12}$ as a function of the TM from Sc to Ni. Desorption energies of outside hydrogen atoms (H_1–H_2, H_3–H_4) are displayed in Figure 4a, and those of the inside hydrogen atoms (H_7–H_8, H_9–H_{10}, H_{11}–H_{12}) are shown in Figure 4b. We note that all calculations were done with the periodic condition using the VASP code, and the local structure was only used to show the atomic positions more clearly.

Generally, doping TMs in $NaAlH_4$ reduces hydrogen desorption energy from the clean, undoped surface. As shown in Figure 4a, desorption energy for outside hydrogen atoms (H_1–H_2 and H_3–H_4) exhibits a minimum at Ti. For H_3,H_4, there is another minimum with a desorption energy of

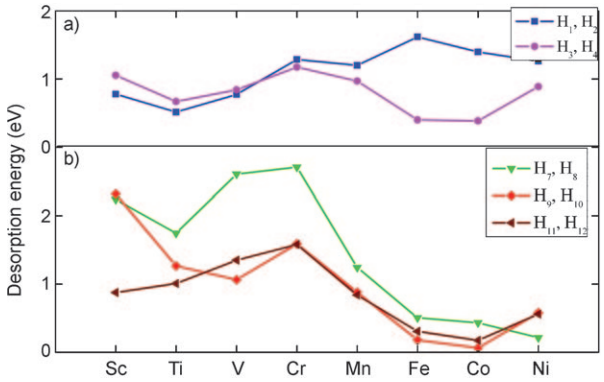

Figure 4. Hydrogen desorption energies from $TMAl_3H_{12}$: a) inside hydrogen atoms; b) outside hydrogen atoms. The numbering of hydrogen atoms as in Figure 2.

0.5 eV for Fe- and Co-doped surfaces. On the other hand, the inside hydrogen atoms (H_7–H_8, H_9–H_{10}, H_{11}–H_{12}) of the Fe-, Co-, and Ni-doped interstitial structures have a very low desorption energy as shown in Figure 4b. In contrast, the desorption energy of the inside hydrogen atoms in the Sc-, Ti-, V-doped structures is relatively high, even higher than the desorption energy (1.382 eV) from the clean surface without dopants. Based on these results, we can conclude that the early TMs (Sc, Ti, V) lead to low desorption energies for outside hydrogen atoms of the interstitial complex structure, whereas the late TMs (Fe, Co, Ni) will cause the inside hydrogen atoms to be desorbed easily. The variation of hydrogen desorption energies from the interstitial structure doped with different TMs can again be understood with the aid of the 18-electron rule. $TMAl_3H_{12}$ is electron-deficient for Sc–V, electron-neutral for Cr, and electron-rich for Mn–Ni. The desorption of inside hydrogen atoms from the complex structures formed with Sc–V will make the structure even more deficient and further away from the required 18 electrons, resulting in even higher desorption energies. On the other hand, the loss of the outside hydrogen atoms will supply electrons to the electron-deficient $TMAl_3H_{12}$ complexes formed with the early TMs (Sc, Ti, V) and make these complexes closer to the required 18 electrons. In the case of Ti, losing one pair of outside hydrogen atoms transforms the original complex into $TiAl_3H_{10}$, which has precisely 18 electrons and corresponds to the minimum of the desorption energy. This is supported by our Bader charge analysis of the $TiAl_3H_{12}$ complex and its product $TiAl_3H_{10}$(1,2) by removing H_1 and H_2, as shown in Table 1. In $TiAl_3H_{12}$, each H atom has a charge of $-0.73\ |e|$. After desorbing H_1 and H_2, the excess electrons associated with them were transferred to Al_1 (55%), Al_2 (15%), and Al_3 (13%). These electrons became available to Ti through Al–H ligands. Only 17% of the charges were distributed to the surrounding atoms.

The above analysis may not seem applicable to Fe–Ni for H_3–H_4 and to Co–Ni for H_1–H_2 at first sight, as these H atoms showed rather low desorption energies. A closer examination of the complex structure revealed that the Al_2

Table 1. Calculated atomic Bader charge in the complexes $TiAl_3H_{10}$(1,2) by removing H_1 and H_2, $TiAl_3H_{12}$, $TiAl_3H_{10}$–H_2, $TiAl_3H_{10}$(7,8) by removing H_7 and H_8. The respective formal valence electron number (Ti:4, Al:3, and H: 1) was used as a reference.

	$TiAl_3H_{10}$(1,2)	$TiAl_3H_{12}$	$TiAl_3H_{10}$–H_2	$TiAl_3H_{10}$(7,8)
Ti	0.92	0.92	0.75	0.80
Al_1	0.41	1.20	1.32	0.88
Al_2	1.81	2.02	1.60	1.63
Al_3	1.85	2.03	1.35	1.65
H_1		−0.75	−0.74	−0.76
H_2		−0.75	−0.74	−0.76
H_3	−0.73	−0.74	−0.75	−0.75
H_4	−0.75	−0.73	−0.73	−0.72
H_5	−0.73	−0.73	−0.72	−0.72
H_6	−0.75	−0.74	−0.72	−0.75
H_7	−0.70	−0.68	−0.16	
H_8	−0.69	−0.68	−0.20	
H_9	−0.71	−0.71	−0.74	−0.65
H_{10}	−0.69	−0.72	−0.70	−0.66
H_{11}	−0.64	−0.64	−0.65	−0.72
H_{12}	−0.71	−0.64	−0.62	−0.71

and Al_3 groups (AlH_4^-) were separated from the TM after H_1–H_2 desorption from the Co- and Ni-doped complex to maintain 18 electrons in the valence shell. This in turn reduces hydrogen desorption energies of H_1–H_2. In fact, desorption of H_3–H_4 from a complex formed with Fe–Ni makes H_7 and H_9 hydrogen atoms displace from inside to outside. These structural changes resulted in less ligands (in the form of Al−H bonds) coordinated to the TM, thus fulfilling the 18-electron requirement. We expect that the structural variations in response to the number of H atoms bonded to the Al atoms play important roles in the catalytic cycle of TM-doped $NaAlH_4$. A cycle between the electron-deficient and electron-rich states facilitates hydrogen desorption/adsorption as well as hydrogen transfer between the local complex structure and the surrounding AlH_4^- units in the doped $NaAlH_4$.

Transition-metal complex with dihydrogen($TMAl_3H_{10}$–H_2): We further analyzed desorption of the inside H atoms by considering the hydrogen desorption process as a stepwise process: the H atoms first recombine on the TM site to form dihydrogen as an intermediate, and the intermediate is then separated from the TM site. These steps will be referred to as recombination(R) and separation(S), respectively, in the subsequent discussion. We illustrated the process for H_7–H_8 desorption in Figure 5. Step R in the upper panel of Figure 5 corresponds to the formation of the $TMAl_3H_{10}$–H_2 intermediate as a result of H_7–H_8 recombination. In step S, the dihydrogen was separated from the complex, resulting in hydrogen desorption. The overall desorption energies of this hydrogen pair were plotted in green as a function of the TM in the lower panel of Figure 5. The energy costs for the recombination and separation steps were also calculated separately and plotted in the figure. A positive value indicates an endothermic process, whereas a negative value corresponds to an exothermic one. Generally, the separation energy contributes dominantly to the overall desorption

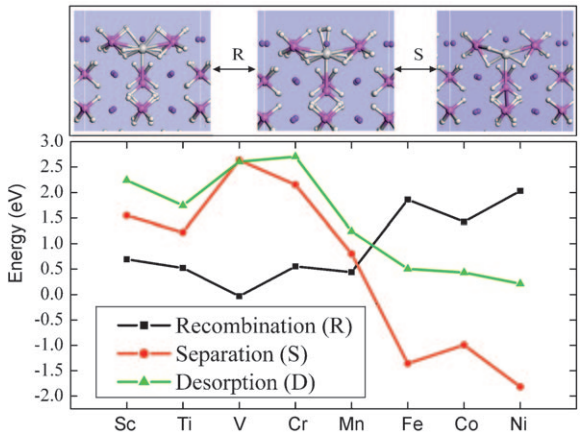

Figure 5. Variation of recombination, separation, and desorption energy of H_7–H_8 in $TMAl_3H_{12}$ with TM.

energy for the structures formed with Sc–Mn. For Fe-, Co-, Ni-doped interstitial structures, the separation of the dihydrogen from the TM site becomes highly exothermic. This trend of separation energy corresponds well with the relatively low recombination energy for early TM complexes and relatively high one for Fe, Co, and Ni

In these complexes, a stretched dihydrogen (by 0.05–0.25 Å from the value for a gas phase H−H bond) binds side-on to the TM with TM···H distances of 1.8–2.1 Å. To establish that the dihydrogen complex, $TMAl_3H_{10}$–H_2, is at a local minimum, we performed a frequency analysis for the $TiAl_3H_{10}$–H_2 structure. The results showed that the complex does not have any imaginary frequencies and, therefore, corresponds to a minimum. The H−H stretching mode has a harmonic frequency of 1738.9 cm^{-1}. The establishment of the dihydrogen complex suggested that a stable intermediate can be formed between the interstitial complex and dihydrogen (H−H).

We further analyzed the Bader charge and the projected LDOS of the $TiAl_3H_{10}$–H_2 complex. The Bader charges of the dihydrogen complex are listed in Table 1 together with those of $TiAl_3H_{12}$ and $TiAl_3H_{10}$(7,8), the product of losing the dihydrogen. The projected LDOS of Ti, $A1_1$, and Al_2 as well as the two H atoms are shown in Figure 6. As a reference, the Bader charges of Al and H in an undisturbed tetrahedral AlH_4^- structure are 2.12 and −0.74 |e|, respectively.

The formation of $TiAl_3H_{10}$–H_2 caused a redistribution of electrons: the electrons associated with H_7 and H_8 atoms in $TiAl_3H_{12}$ are now transferred to Al_2 and Al_3. This charge transfer results from dihydrogen formation on the Ti site and caused Al_2 and Al_3 to become less positively charged than the corresponding atoms in $TiAl_3H_{12}$. Consequently, the attractive interactions between these Al atoms and the remaining H atoms were reduced and led to weakened Al_2–H and Al_3–H bonds. The charge transfer from the Al atoms to the H atoms was facilitated by the Ti atom, as the projected LDOS peaks of −0.25 and −0.45 eV of Al_2 and Al_3 originated from the corresponding $d_{x^2-y^2}$ and d_{xy} orbitals of

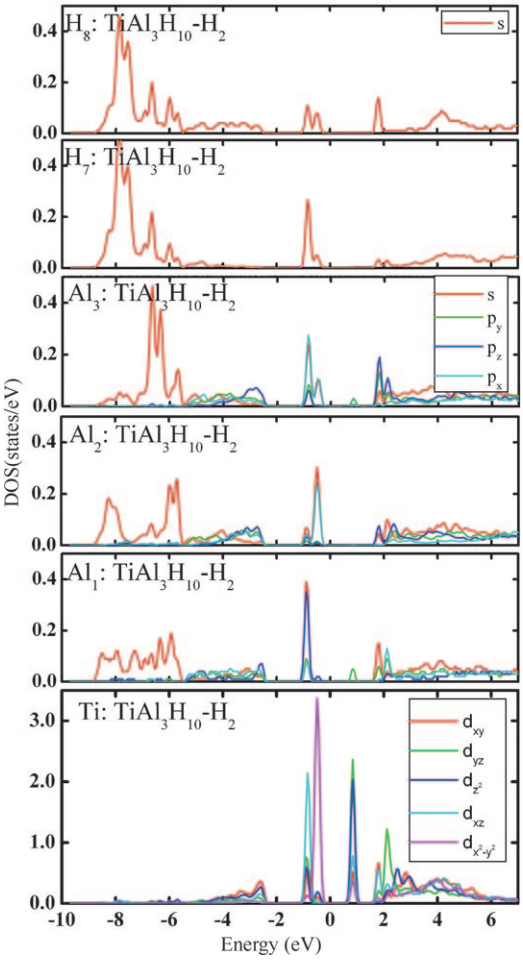

Figure 6. Projected local density-of-states of Ti, Al_1, Al_2, Al_3, H_7, and H_8 in dihydrogen complex $TiAl_3H_{10}$–H_2. The numbering of the Al and H atoms as in Figure 2.

Ti. The variation of the charge on Ti in complexes is relatively small, from 0.93 |e| in $TiAl_3H_{12}$ to 0.75 |e| in $TiAl_3H_{10}$–H_2, and then, to 0.80 |e| in $TiAl_3H_{10}$(7,8), as shown in Table 1. The backdonation from Ti shown in the energy range of −2 to 0 eV in the projected LDOS (Figure 6) can be attributed to the π-type orbital interactions between the d_{xz} orbital of Ti and the σ* orbital of H_7–H_8. In addition, there are significant overlaps between the $d_{x^2-y^2}$ orbital of Ti and the σ* orbital of the dihydrogen. As shown in Table 1, the dihydrogen is negatively charged, with a total charge of −0.36 |e|. According to Kubas,[41] these electrons can be attributed to the backdonation from the filled d orbitals of Ti to the antibonding orbital (σ*) of H–H. Such interactions play important roles in stabilizing the dihydrogen complex and further activating the H–H bond. The almost equal amount of charge on the two H atoms indicates both recombination and dissociation are homolytic. The lower recombination energy with early TMs shown in Figure 5b is a result of the stronger backdonation. Other contributions to the projected LDOS in the same energy range originate from the interactions between $d_{x^2-y^2}$ of Ti and p_x of Al_2, as well as between d_{z^2} of Ti and p_z of Al_1.

General discussions: Extensive experimental investigations have been performed to characterize Ti-doped $NaAlH_4$ and to determine the active species responsible for the accelerated dehydrogenation and rehydrogenation. Although Ti–Al alloys, in particular $TiAl_3$, have been identified in both dehydrogenated and hydrogenated samples, there was no consensus on the role played by the alloys in hydrogen release/uptake.[12,27,34,60–63] The $TiAl_3$ alloy has been doped directly in $NaAlH_4$ and was found to be substantially less effective on the dehydrogenation/rehydrogenation kinetics than the Ti halides.[21,64] These results indicated that $TiAl_3$, in either crystalline or cluster form, does not achieve the same level of catalytic effect as the Ti halides. Many experimental studies suggested that highly dispersed Ti in a predominately Al phase might play an important role in hydrogen desorption and sorption processes,[34,65–67] whereas a Ti–Al alloy phase may be formed but acted largely as a spectator rather than catalyst. On the other hand, the interstitial complex structures that we identified for Ti and Sc previously and examined here for other TM elements can be the catalytically active centers.[32,33,48] In fact, experimental studies have confirmed the existence of the interstitial structure in Ti-doped $NaAlH_4$.[34] The role of a Ti-Al-H species, including TiH_2, has been discussed based on the ^{27}Al and ^{1}H MAS NMR spectroscopy, and ^{27}Al multiple quantum studies of Ti-doped $NaAlH_4$ by Herberg et al.[62]

The effectiveness of various TM elements as catalysts can be analyzed by revisiting Figure 5. Figure 5b shows the overall desorption energy as well as the recombination and separation energy of H_7–H_8 for different TMs. To form $TMAl_3H_{10}$–H_2 from the $TMAl_3H_{12}$ complex, the recombination energy for Sc–Mn is significantly lower than that for Fe–Ni. In contrast, the separation energy of dihydrogen from the $TMAl_3H_{10}$–H_2 complex of electron-rich Fe–Ni is negative, indicating an exothermic process. We also calculated the recombination and separation energies of $ScAl_3H_6$ and $TiAl_3H_6$ obtained by removing all outside hydrogen atoms (see Table 2). These complexes are electron-rich due to the loss of outside hydrogen. The recombination energy from the complexes is significantly higher than in the corresponding $TMAl_3H_{12}$, whereas the separation energy is relatively low, similar to the electron-rich complex formed with the Fe–Ni systems. All these results indicate that the electron-deficient complexes have low recombination energies and high separation energies, whereas the electron-rich complexes exhibit opposite trends. On the basis of the above analyses, we suggest the following mechanism in TM-doped

Table 2. Recombination, separation, and desorption energies of $ScAl_3H_6$ and $TiAl_3H_6$ complexes.

Species	Recombination	Separation	Desorption
$ScAl_3H_6$	1.444	0.343	1.787
$TiAl_3H_6$	1.123	0.622	1.745

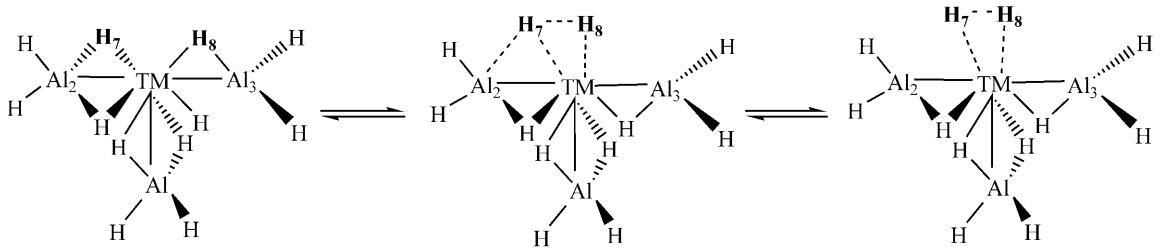

Scheme 1. A σ-bond metathesis process catalyzed by TM for the exchange of ligands, that is, Al–H for H–H.

$NaAlH_4$: The electron-deficient complexes formed with the early TMs go through a series of steps, starting with inside hydrogen recombination→outside hydrogen desorption→inside hydrogen separation. The process is accompanied by an oscillation between electron-deficient and electron-rich states of the complexes. On the other hand, for an electron-rich complex, both inside hydrogen recombination and outside hydrogen desorption occur with a high energy cost. Therefore, late TMs are not efficient as catalysts for hydrogen release/uptake from $NaAlH_4$.

As shown in Figure 3, there is a much stronger backdonation from Ti to Al_1 than to Al_2 or Al_3 in the $TiAl_3H_{12}$ complex structure. This is also reflected in the Bader charge values listed in Table 1: the charge on Al_1 was reduced to 1.2 |e|, whereas that on Al_2 only decreased to 2.0 |e|. Projected LDOS analysis showed that electron transfer between Ti and Al_1 involved the d_{z^2} of Ti and the p_z and s orbitals of Al_1. As we reported previously, the d_{z^2} orbital also contributed to the formation of dihydrogen.[32] In addition, the projected LDOS showed that the $d_{x^2-y^2}$ orbital mixed with the antibonding orbitals of the Al_2 and Al_3 units, causing the Al_2–H_7 and Al_3–H_8 bonds to break more easily. Therefore, the d_{z^2} and $d_{x^2-y^2}$ orbitals of Ti are critical to dihydrogen formation and are involved in transferring hydrogen from AlH_4^- to Ti. The formation of dihydrogen led to the depopulation of the d_{z^2} orbital and the filling of the d_{xy} orbital, as indicated in the projected LDOS of Ti in Figure 6. During dehydrogenation, such electron redistribution facilitates H–H bond formation and stabilizes the dihydrogen intermediate. In the process of forming dihydrogen, the electron transfer involves both donation and backdonation: the electrons were donated to the d_{xz} orbital of Ti from the s orbitals of hydrogen atoms, and then backdonated from the filled d_{xz} and $d_{x^2-y^2}$ orbitals to the antibonding orbitals of the Al_2 and Al_3 units. Furthermore, desorption of the negatively charged dihydrogen left its electrons to fill the $d_{z^2}$and $d_{x^2-y^2}$ orbitals, as shown in the projected LDOS in Figure 6 and those provided in the Supporting Information. Such charge transfer processes are expected to continue for $TiAl_3H_{10}$ and subsequent products, until the product cannot sustain the dehydrogenation process. Therefore, the interaction between Ti-d_{z^2} and σ* of the Al_1 unit is critical to hydrogen transfer and dihydrogen formation, whereas the interaction between Ti-d_{xz} as well as Ti-$d_{x^2-y^2}$ and the antibonding orbitals of Al_2 and Al_3 units stabilizes the dihydrogen intermediate.

The exchange of ligands, that is, Al–H for H–H, by the TM can be considered as a σ-bond metathesis process catalyzed by TM.[68–70] As shown in Scheme 1: the first step involves the breaking of an Al–H bond from the $TMAl_3H_{12}$ complex and the formation of a four-membered intermediate (TM-Al_2–H_7–H_8). This step is followed by the formation of the dihydrogen coordinated with the TM by breaking the Al_2–H_7 bond.

Our discussions so far have been focused on the effect of the TM on the dehydrogenation of $NaAlH_4$. One question that remains to be answered is how the complex structure fits in the overall mechanism of hydrogenation. As shown in Scheme 1, the reverse process started from the dihydrogen complex and reaches the $TMAl_3H_{12}$ complex structure through the four-membered intermediate state. We can get some further understanding of the hydrogenation process by examining the variations in Bader charges from $TiAl_3H_{10}$-(7,8), $TiAl_3H_{10}$–H_2, and then to $TiAl_3H_{12}$ (see Table 1). In all three states, the charge on Ti is almost constant. However, there is a significant amount of charge transferred between Al and H. In the first step of hydrogenation, from $TiAl_3H_{10}$-(7,8) to $TiAl_3H_{10}$–H_2, electrons are transferred from Al_1 to the σ* orbital of H_2 to activate the H–H bond and stabilize the dihydrogen complex through the Ti–d_{z^2} orbitals. As discussed above, the interaction between the d_{z^2} orbital and the Al_1–σ* orbital facilitates dihydrogen complex formation. The second step, from the dihydrogen complex to $TiAl_3H_{12}$, also involves electron transfer from Al_2 and Al_3 to H. Clearly, Ti–$d_{x^2-y^2}$ and Ti–d_{xz} orbitals can interact with not only the σ* orbitals of Al_2 and Al_3 units, but also the σ* orbital of H_7–H_8. Once sufficient electrons are transferred from Al_2 and Al_3 to H–H through Ti–$d_{x^2-y^2}$ and Ti–d_{xz}, the H–H bond will be broken, resulting in $TiAl_3H_{12}$ formation.

The importance of electron backdonation from Ti to H_2/H in the hydrogenation process has also been demonstrated in recent studies by Chaudhuri et al.[23,71] Starting from a Ti-doped Al(001) surface, these authors studied the hydrogenation process and proposed that the first step of hydrogenation involves breaking the molecular H–H bond, followed by migration of H to the Al sites. They showed that a special local arrangement in which two Ti atoms occupy next-nearest-neighbor positions facilitates electron transfer from 3d orbitals of Ti to the σ* orbital of H–H. Our analyses indicated that the occupation of Ti d orbitals was maintained at an almost constant level by the electron transfer from Al to Ti.

Therefore, we expect the ability to balance accepting in and backdonating electrons from its d orbitals to be an important characteristic of a candidate as a catalyst for hydrogen release/uptake from $NaAlH_4$. Our analyses are consistent with the experimental observations that showed early TMs, in particular, Sc and Ti, exhibited superior catalytic properties.[29–31]

Conclusion

We studied the energetics and structures of TM-doped $NaAlH_4$(001) surfaces using the DFT-PBE method with plane-wave basis set and PAW potentials. On the basis of our results, we conclude:

1) The stability of the structures formed upon doping the 3d TM elements was found to follow the 18-electron rule. The interstitial complex structure, $TMAl_3H_{12}$, in which the TM atom occupies the interstitial position formed from three AlH_4^- units was identified to be the most stable structure for Sc–Co.
2) The interstitial structures formed with Sc–V are electron-deficient and those with Mn–Ni are electron-rich. The electron-deficient $TMAl_3H_x$ complexes approach the 18-electron state by coordinating with the surrounding Al–H bonds and dihydrogen, or by losing "outside" hydrogen atoms through desorption. On the other hand, the electron-rich complexes tend to lose the excess electrons by either releasing AlH_x or desorbing the "inside" hydrogen.
3) The early TMs are more efficient at reducing the hydrogen desorption energy as well as at activating the H–H bond than the late TMs. The hydrogen release/uptake process can be considered as an exchange of σ-bond ligands (H–H for Al–H) in the $TMAl_3H_{12}$ complex. The mechanism is consistent with the metathesis process involving σ bonds. The balance between the ability of accepting electrons in and backdonating electrons from the d orbitals of the early TMs made them ideal candidates as catalysts for hydrogen release/uptake.

Computational Methods

Periodic DFT calculations including spin-polarization have been carried out using the VASP code.[72,73] The electron-ion interactions were described by using the projector augmented wave (PAW) potential, and the valence electrons of Al $3s^23p^1$, Na $2p^63s^1$, H $1s^1$, and TMs $3d^n4s^m$ were treated explicitly with a plane-wave cutoff energy of 400 eV. The nonlocal exchange-correlation energy was calculated with the PBE functional.[74] The surface Brillouin zone was sampled with the K-points generated by the Monkhorst–Pack scheme with a space less than 0.05 $Å^{-1}$.[75] Similar parameters have been used in our previous calculations and were shown to give converged results.[32,33,48]

Slabs with six-layer metal atoms (Al or Na) consisting of 24 $NaAlH_4$ units were constructed on the basis of the relaxed bulk structure to simulate the surfaces. The dimension of the super-cell to simulate the (001) surface is $9.96 \times 9.96 \times 27.8$ $Å^3$, leaving a vacuum space of about 15 Å in the z direction. The geometries of the clean slab were optimized by using the quasi-Newton or conjugate-gradient method as implemented in VASP. A Gaussian smearing with a width of 0.1 eV was employed to improve the convergence of the electronic self-consistent cycles. A calculation was considered as converged when the changes in energy and forces were less than 1.0×10^{-6} eV and 0.05 eV $Å^{-1}$, respectively. The Al and Na atoms in the bottom three layers of the slab were fixed at their corresponding bulk positions during the relaxation. Those in the top three layers as well as all the hydrogen atoms were allowed to relax according to the calculated Hellman–Feynman forces. We would like to point out that zero-point energy corrections were not included in the reported energetics.

Acknowledgements

This work was supported by the U. S. Department of Energy, Contract No. DE-FG02-05ER46231 and the American Chemical Society Petroleum Research Fund.

[1] L. Schlapbach, A. Züttel, *Nature* **2001**, *414*, 353–358.
[2] M. Felderhoff, C. Weidenthaler, R. von Helmot, U. Eberle, *Phys. Chem. Chem. Phys.* **2007**, *9*, 2643–2653.
[3] S. Orimo, Y. Nakamura, J. R. Eliseo, A. Züttel, C. M. Jensen, *Chem. Rev.* **2007**, *107*, 4111–4132.
[4] T. J. Clark, K. Lee, I. Manners, *Chem. Eur. J.* **2006**, *12*, 8634–8648.
[5] P. Vermeulen, E. F. M. J. van Thiel, P. H. L. Notten, *Chem. Eur. J.* **2007**, *13*, 9892–9898.
[6] N. L. Rosi, J. Eckert, M. Eddaoudi, D. T. Vodak, J. Kim, M. O'Keeffe, O. M. Yaghi, *Science* **2003**, *300*, 1127–1129.
[7] H. Li, Y. Tao, Q. Yu, X. Bu, H. Sakamoto, S. Kitagawa, *Chem. Eur. J.* **2008**, *14*, 2771–2776.
[8] Y. Liu, J. F. Eubank, A. J. Cairns, J. Eckert, V. C. Kravtsov, R. Luebke, M. Eddaoudi, *Angew. Chem.* **2007**, *119*, 3342–3347; *Angew. Chem. Int. Ed.* **2007**, *46*, 3278–3283.
[9] B. Bogdanovic, M. Schwickardi, *J. Alloys Compd.* **1997**, *253–254*, 1–9.
[10] O. Kircher, M. Fichtner, *J. Alloys Compd.* **2005**, *404–406*, 339–342.
[11] J. Wang, A. D. Ebner, J. A. Ritter, *J. Phys. Chem. B* **2006**, *110*, 17353–17358.
[12] H. W. Brinks, M. Sulic, C. M. Jensen, B. C. Hauback, *J. Phys. Chem. B* **2006**, *110*, 2740–2745.
[13] D. Sun, S. S. Srinivasan, T. Kiyobayashi, N. Kuriyama, C. M. Jensen, *J. Phys. Chem. B* **2003**, *107*, 10176–10179.
[14] S. S. Srinivasan, H. W. Brinks, B. C. Hauback, D. Sun, C. M. Jensen, *J. Alloys Compd.* **2004**, *377*, 283–289.
[15] D. Pukazhselvan, M. Sterlin Leo Hudson, B. K. Gupta, M. A. Shaz, O. N. Srivastava, *J. Alloys Compd.* **2007**, *439*, 243–248.
[16] O. M. Lovvika, O. Swang, *J. Alloys Compd.* **2005**, *404–406*, 757–761.
[17] P. Wang, C. M. Jensen, *J. Alloys Compd.* **2004**, *379*, 99–102.
[18] J. M. Bellosta von Colbe, M. Felderhoff, B. Bogdanovic, F. Schüth, C. Weidenthaler, *Chem. Commun.* **2005**, 4732–4734.
[19] B. Bogdanovic, R. A. Brand, A. Marjanovic, M. Schwickardi, J. Tolle, *J. Alloys Compd.* **2000**, *302*, 36–58.
[20] D. Sun, S. S. Srinivasan, G. Chen, C. M. Jensen, *J. Alloys Compd.* **2004**, *373*, 265–269.
[21] J. Shim, G. Lee, Y. W. Cho, *J. Alloys Compd.* **2006**, *417*, 69–71.
[22] V. P. Balema, J. M. Wiench, K. W. Dennis, M. Pruski, V. K. Pecharsky, *J. Alloys Compd.* **2001**, *329*, 108–114.
[23] S. Chaudhuri, J. Graetz, A. Ignatov, J. J. Reilly, J. T. Muckerman, *J. Am. Chem. Soc.* **2006**, *128*, 11404 –11415.
[24] R. Gremauda, A. Borgschultea, W. Lohstroha, H. Schreudersa, A. Zuttela, B. Dama, R. Griessena, *J. Alloys Compd.* **2005**, *404–406*, 775–778.
[25] Y. Nakamura, A. Fossdal, H. W. Brinks, B. C. Hauback, *J. Alloys Compd.* **2005**, *404-406*, 274–278.

[26] T. Vegge, *Phys. Chem. Chem. Phys.* **2006**, *8*, 4853–4861.
[27] J. Graetz, J. J. Reilly, J. Johnson, A. Y. Ignatov, T. A. Tyson, *Appl. Phys. Lett.* **2004**, *85*, 500–502.
[28] O. M. Løvvik, S. M. Opalka, *Phys. Rev. B* **2005**, *71*, 054103.
[29] D. L. Anton, *J. Alloys Compd.* **2003**, *356–357*, 400–404.
[30] B. Bogdanovic, M. Felderhoff, A. Pommerin, F. Schüth, N. Spielkamp, *Adv. Mater.* **2006**, *18*, 1198–1201.
[31] T. Wang, J. Wang, A. D. Ebner, J. A. Ritter, *J. Alloys Compd.* **2006**, *450*, 293–300.
[32] J. Liu, Q. Ge, *Chem. Commun.* **2006**, 1822–1824.
[33] J. Liu, Q. Ge, *J. Phys. Chem. B.* **2006**, *110*, 25863–25868.
[34] C. P. Balde, H. A. Stil, A. M. J. van der Ederden, K. P. de Jong, J. H. Bitter, *J. Phys. Chem. B* **2007**, *111*, 2797–2802.
[35] J. Íñiguez, T. Yildirim, T. J. Udovic, M. Sulic, C. M. Jensen, *Phys. Rev. B* **2004**, *70*, 060701.
[36] C. M. Araújo, R. Ahuja, J. M. Osorio Guillén, P. Jena, *Appl. Phys. Lett.* **2005**, *86*, 251913.
[37] D. M. P. Mingos, *J. Organomet. Chem.* **2004**, *689*, 4420–4436.
[38] G. J. Kubas, *J. Acc. Chem. Res.* **1988**, *21*, 120.
[39] G. J. Kubas, *Metal dihydrogen and sigma-bond complexes: structure, theory, and reactivity*, Kluwer Academic, New York, **2001**.
[40] F. Maseras, A. Lleedos, E. Clot, O. Eisenstein, *Chem. Rev.* **2000**, *100*, 601–636.
[41] G. J. Kubas, *Science* **2006**, *314*, 1096.
[42] S. A. Shevlin, Z. X. Guo, *Appl. Phys. Lett.* **2006**, *89*, 153104.
[43] Y. Zhao, Y. Kim, A. C. Dillon, M. J. Heben, S. B. Zhang, *Phys. Rev. Lett.* **2005**, *94*, 155504.
[44] Q. Sun, Q. Wang, P. Jena, Y. Kawazoe, *J. Am. Chem. Soc.* **2005**, *127*, 14582–14583.
[45] T. Yildirim, J. Iñiguez, S. Ciraci, *Phys. Rev. B* **2005**, *72*, 153403.
[46] L. Gagliardi, P. Pyykkö, *J. Am. Chem. Soc.* **2004**, *126*, 15014–15015.
[47] B. Kiran, A. K. Kandalam, P. Jena, *J. Chem. Phys.* **2006**, *124*, 224703.
[48] J. Liu, Q. Ge, *J. Alloys Compd.* **2007**, *446–447*, 267–270.
[49] C. M. Araújo, S. Li, R. Ahuja, P. Jena, *Phys. Rev. B* **2005**, *72*, 165101.
[50] J. Íñiguez, T. Yildirim, *Appl. Phys. Lett.* **2005**, *86*, 103109.
[51] A. Leon, O. Kircher, J. Rothe, M. Fichtner, *J. Phys. Chem. B* **2004**, *108*, 16372–16376.
[52] J. Chatt, L. A. Duncanson, *J. Chem. Soc.* **1953**, 2939.
[53] J. S. Dewar, *Bull. Soc. Chim. Fr.* **1951**, *18*, c79.
[54] G. Frenking, N. Fröhlich, *Chem. Rev.* **2000**, *100*, 717–774.
[55] G. Frenking, U. Pidum, *J. Chem. Soc. Dalton Trans.* **1997**, 1653–1663.
[56] G. Frenking, M. Solà, S. F. Vyboishchikov, *J. Organomet. Chem.* **2005**, *690*, 6178–6204.
[57] M. Torrent, M. Solà, G. Frenking, *Chem. Rev.* **2000**, *100*, 439–494.
[58] A. Peles, J. A. Alford, Z. Ma, L. Yang, M. Y. Chou, *Phys. Rev. B* **2004**, *70*, 165105.
[59] B. Hammer, J. K. Nørskov, *Adv. Catal.* **2000**, *45*, 71.
[60] M. Felderhoff, K. Klementiev, W. Grünert, B. Spliethoff, B. Tesche, J. M. Bellosta von Colbe, B. Bogdanovic, M. Härtel, A. Pommerin, F. Schüth, C. Weidenthaler, *Phys. Chem. Chem. Phys.* **2004**, *6*, 4369–4374.
[61] H. W. Brinks, B. C. Hauback, S. S. Srinivasan, C. M. Jensen, *J. Phys. Chem. B* **2005**, *109*, 15780–15785.
[62] J. L. Herberg, R. S. Maxwell, E. H. Majzoub, *J. Alloys Compd.* **2006**, *417*, 39–44.
[63] E. H. Majzoub, J. L. Herberg, R. Stumpf, S. Spangler , R. S. Maxwell, *J. Alloys Compd.* **2005**, *394*, 265–270.
[64] X.-D. Kang, P. Wang, X. P. Song, X. D. Yao, G. Q. Lu, H.-M. Cheng, *J. Alloys Compd.* **2006**, *424*, 365–369.
[65] C. Weidenthaler, A. Pommerin, M. Felderhoff, B. Bogdanovic, F. Schüth, *Phys. Chem. Chem. Phys.* **2003**, *5*, 5149–5153.
[66] A. G. Haiduc, H. A. Stil, M. A. Schwarz, P. Paulus, J. J. C. Geerlings, *J. Alloys Compd.* **2005**, *393*, 252–263.
[67] A. Leon, O. Kircher, M. Fichtner, J. Rothe, D. Schild, *J. Phys. Chem. B* **2006**, *110*, 1192–1200.
[68] Y. Musashi, S. Sakaki, *J. Am. Chem. Soc.* **2000**, *122*, 3867–3877.
[69] L. Ding, P. Marshall, *J. Am. Chem. Soc.* **1992**, *114*, 5754–5758.
[70] T. Ziegler, E. Folga, A. Berces, *J. Am. Chem. Soc.* **1993**, *115*, 636–646.
[71] S. Chaudhuri, J. T. Muckerman, *J. Phys. Chem. B.* **2005**, *109*, 6952–6957.
[72] G. Kresse, J. Furthmüller, *Comput. Mater. Sci.* **1996**, *6*, 15–50.
[73] G. Kresse, J. Furthmüller, *Phys. Rev. B* **1996**, *54*, 11169.
[74] J. P. Perdew, J. A. Chevary, S. H. Vosko, K. A. Jackson, M. R. Pederson, D. J. Singh, C. Fiolhais, *Phys. Rev. B* **1992**, *46*, 6671.
[75] H. J. Monkhorst, J. D. Pack, *Phys. Rev. B* **1976**, *13*, 5188.

Received: May 29, 2008
Revised: August 30, 2008
Published online: December 29, 2008

